Available online at www.sciencedirect.com
ScienceDirect
International Journal of Heat and Fluid Flow 29 (2008) 568–578
International Journal of HEAT AND FLUID FLOW
www.elsevier.com/locate/ijhff

Effects of an adverse pressure gradient on a turbulent boundary layer

Joung-Ho Lee, Hyung Jin Sung *

Department of Mechanical Engineering, KAIST,
373-1, Guseong-dong Yuseong-gu, Daejeon 305-701, Republic of Korea

Received 16 November 2007; received in revised form 19 January 2008; accepted 24 January 2008
Available online 20 March 2008

Abstract

Direct numerical simulations were performed to investigate the effects of an adverse pressure gradient (APG) on a turbulent boundary layer. A fully implicit fractional step method was employed to simulate the flows. Equilibrium APG flows were established using a power-law free-stream distribution, $U_\infty \sim x^m$. The streamwise length from the inlet was made sufficiently long that the change in free-stream velocity associated with the APG did not influence the main stream. The flow with zero pressure gradient (ZPG) was also simulated and compared with the APG flows. The spatially developing characteristics of the turbulence stresses in the non-equilibrium APG flows were carefully examined. The instantaneous flow fields and vorticity fluctuations were analyzed to characterize the response of the outer turbulence to an APG. The present numerical results showed that the mean flows are greatly affected by an APG, and the coherent structures in the outer layer of the APG flows were more activated than those in the ZPG flow which may be attributed to increased turbulence intensities, shear stresses and pressure fluctuations in the APG systems. Examination of the Reynolds stress budget revealed that the energy redistribution was enhanced in the outer layer of the APG flows compared to the ZPG flow.

Keywords: Adverse pressure gradient; Turbulent boundary layer; Direct numerical simulation; Budget of Reynolds stress; Vortex identification

1. Introduction

Flows subjected to an adverse pressure gradient (APG) occur in numerous engineering applications, including diffusers, turbine blades and the trailing edges of airfoils. The performance of such flow devices is greatly affected by the presence of an APG. If a turbulent boundary layer flow encounters a large APG, the flow becomes unstable and, if the APG is sufficiently large, separates from the surface. Such separation almost always has negative consequences such as drag reduction and loss of heat transfer. Thus, it is of practical importance to investigate the effects of APGs on turbulent boundary layers.

Many important features of APG flows are quite well understood. In general, as the magnitude of an APG increases, the mean velocity profile develops a large wake region and the turbulent kinetic energy decreases in the near-wall region. Nagano et al. (1993) suggested that this near-wall reduction in turbulent kinetic energy is due to a decrease in the production of turbulent kinetic energy. On the other hand, it is not certain that the standard logarithmic law of the wall holds in APG flows. Skåre and Krogstad (1994) and Bernard et al. (2003) observed that the law of the wall is valid for higher Reynolds number APG flows and for the decelerating flow around an airfoil, respectively. In contrast, Nagano et al. (1993) showed that the logarithmic region is shifted below the standard logarithmic law profile for turbulent boundary layer flows where the pressure gradient is maintained at a nearly constant positive value. This shift was also observed in the APG recovery section of a backward-facing step flow

* Corresponding author. Tel.: +82 42 869 3027; fax: +82 42 869 5027.
E-mail address: hjsung@kaist.ac.kr (H.J. Sung).

0142-727X/$ - see front matter © 2008 Elsevier Inc. All rights reserved.
doi:10.1016/j.ijheatfluidflow.2008.01.016

(Le et al., 1997) and in other decelerating flows (Spalart and Watmuff, 1993; Debisschop and Nieuwstadt, 1996). Nagano et al. (1993) found that the turbulence intensity profiles in the outer region of APG flows collapse onto a single curve when normalized by the inlet free-stream velocity. Coleman et al. (2003) also examined the outer layer turbulence of a temporally developing flow; however, their findings cast doubt on whether the velocity fluctuations along the streamlines in the outer region are conserved. The effects of an APG on the mean velocity and the outer layer dynamics depend on both the characteristics of the APG and the geometrical shape of the surface. Hence, to isolate the effect of an APG, it is necessary to consider a flat plate surface.

Turbulent flows with an APG have been regarded as being among the most difficult flows to predict using turbulence models (Wilcox, 1993). The Reynolds stress equations, which are the basis for closure of the Reynolds averaged Navier–Stokes equations, include several terms that must be modeled (e.g., pressure–strain tensor and dissipation). Since direct numerical simulation (DNS) can provide accurate information directly, DNS findings would be instructive for the improvement of turbulence models. The major difficulty in simulating a spatially evolving turbulent boundary layer with an APG is imposing the conditions of free-stream flows and realistic turbulent inflows. Since there is no systematic way to choose boundary conditions that result in a specific pressure distribution, an iterative procedure is required (Na and Moin, 1998). For these reasons, only a limited number of DNS studies of APG flows over a flat plate have been conducted. Moreover, previous DNSs have failed to reproduce some of the experimental findings for APG flows, such as the existence of inward turbulent energy transport which is the opposite of that observed in systems with a zero pressure gradient (ZPG), and the development of a distinct outer peak in the streamwise turbulence intensity (Bradshaw, 1967; Cutler and Johnston, 1989; Nagano et al., 1993; Skåre and Krogstad, 1994). Clauser (1954) suggested a new class of equilibrium boundary layer with an APG, in which the ratio of the pressure gradient force to the wall shear force remains constant. The mean velocity profiles in an equilibrium boundary layer at different streamwise locations show similarity when properly scaled. Townsend (1961) and Mellor and Gibson (1966) showed that an approximate equilibrium flow is obtained when the variation of free-stream velocity in the streamwise direction has the form of a power-law relation $U_\infty \sim x^m$, analogous to Falkner–Skan laminar flow. Hence a power-law relation is employed in the present study. This is valuable from the viewpoint of numerical simulation since the free-stream boundary condition can be applied directly and the strength of the APG can be controlled simply by adjusting the magnitude of m.

In the present study, DNSs of spatially developing turbulent boundary layer flows subjected to several APGs were performed to elucidate the effects of an APG on a turbulent boundary layer. A schematic diagram of the flow configuration is shown in Fig. 1. The Reynolds number was varied in the range $Re_\theta = 300$–1500. To investigate the effects of an APG, simulations were performed using three values of $m = -0.075$, -0.15 and -0.2, representing mild, moderate and strong APGs, respectively. For comparison, the ZPG flow ($m = 0$) was also simulated. The evolutions of turbulence intensity and Reynolds stress in a non-equilibrium turbulent boundary layer were examined. Instantaneous flow fields and vorticity fluctuations were analyzed to characterize the response of the outer layer turbulence to the APG. Finally, the budgets of the Reynolds stress equations were examined to improve turbulence models.

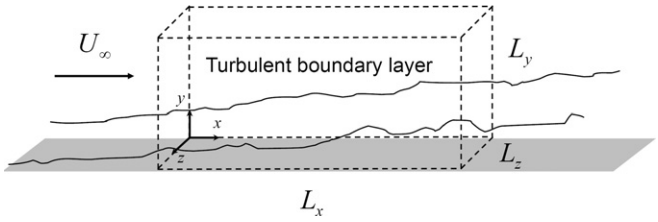

Fig. 1. Schematic diagram of computational domain.

2. Computational details

For an incompressible flow, the non-dimensional governing equations are

$$\frac{\partial u_i}{\partial x_i} = 0, \tag{1}$$

$$\frac{\partial u_i}{\partial t} + \frac{\partial}{\partial x_j} u_i u_j = -\frac{\partial p}{\partial x_i} + \frac{1}{Re}\frac{\partial}{\partial x_j}\frac{\partial u_i}{\partial x_j}, \quad i = 1, 2, 3, \tag{2}$$

where x_i are the Cartesian coordinates, p is the pressure, u_i are the corresponding velocity components, and Re is the Reynolds number. All variables are non-dimensionalized by the momentum thickness θ_{in} and free-stream velocity U_0 at the inlet.

The numerical schemes used in the present work were similar to those of Lee and Sung (2005). The governing equations were integrated in time using the fractional step method with the implicit velocity decoupling procedure proposed by Kim et al. (2002). The computational time step is $\Delta t^+ \approx 0.2$ in wall units. Under this approach, the terms are first discretized in time using the Crank–Nicolson method, and then the coupled velocity components in the convection terms are decoupled using the implicit velocity decoupling procedure. The decoupled velocity components are solved without iteration. Because the implicit decoupling procedure relieves the Courant–Friedrichs–Lewy restriction, the computation time is reduced significantly. The overall accuracy in time is second-order. All of the terms are resolved with a second-order central difference scheme in space with a staggered mesh. Details regarding the numerical algorithm can be found in the paper of Kim et al. (2002).

DNSs of a turbulent boundary layer with an APG were performed by means of a Message Passing Interface (MPI) parallel computation using 64 CPUs of a supercomputer (IBM p690+). The domain size in the streamwise direction was sufficiently long to reach from a zero pressure gradient to an equilibrium APG flow. The domain size in the wall-normal direction was chosen to be about 1.5–2 times the boundary layer thickness at the exit plane of the computational domain. The domain size in the spanwise direction was confirmed to be adequate based on the convergence of the spanwise correlation to zero at this domain size. The grid spacing was uniform in the streamwise and spanwise directions and the grid points in the wall-normal direction were clustered according to a hyperbolic tangent distribution. The domain size and mesh resolution used in the present DNSs are summarized in Table 1. Time-dependent ZPG turbulent inflow data at the inlet were generated based on the method of Lund et al. (1998). The Reynolds numbers at the inlet were 300 for the APG flows and 1410 for the ZPG flow. The convective boundary condition of form $(\partial u/\partial t)+c(\partial u/\partial x)=0$, where c is the local bulk velocity, was applied at the exit; this boundary condition allows propagating vortex structure to exit the domain with minimum distortion. The no-slip condition was imposed at the solid wall. Periodic boundary conditions were applied in the spanwise direction.

The free-stream velocity U_∞ along the upper boundary of the computational domain was prescribed as

$$u = U_\infty(x) = \begin{cases} U_0 & \text{for } x < 0, \\ U_0\left(1-\frac{x}{x_0}\right)^m & \text{for } x > 0, \end{cases} \qquad \frac{\partial v}{\partial y} = -\frac{\partial u}{\partial x}, \qquad \frac{\partial w}{\partial y} = 0. \tag{3}$$

where the streamwise location x_0 and m for defining the free-stream velocity U_∞ are given in Table 1. Four cases ($m=0$, -0.075, -0.15 and -0.2) were chosen (Fig. 2), which correspond to ZPG, and mild, moderate and strong APGs, respectively. In simulations of an APG, a stable equilibrium flow will be obtained only if the streamwise distance from the inlet to where the free-stream velocity begins to change is sufficiently long. This is because APG flows are very sensitive to upstream conditions and the pressure disturbance caused by the change in the free-stream velocity propagates upstream farther than is the case in systems with other types of pressure gradient (Na and Moin, 1998). Na and Moin (1998) and Inman and Bradshaw (1981) indicated that the transient distance needed is about 20 boundary layer thicknesses. In the present study, the transient distance was about 20 times the boundary layer thickness for $m=-0.075$ and -0.15, and about 30 times for $m=-0.2$. To ascertain the reliability and accuracy of the present numerical simulations, we compared the turbulence statistics for the ZPG case ($m=0$) with the experimental data of DeGraaff and Eaton, 2000 (see Figs. 6 and 8). The mean velocity and turbulence intensities are in good agreement with those of DeGraaff and Eaton, 2000.

Table 1
Numerical parameters

m	0	−0.075	−0.15	−0.20
L_x	240	1600	1600	1600
L_y	30	80	80	120
L_z	40	80	80	160
N_x	1025	2049	2049	2049
N_y	161	121	121	161
N_z	513	257	257	513
Δx^+	15	12.5	12.5	12.5
$\Delta y_{\min}{}^+$	0.2	0.17	0.17	0.17
$\Delta y_{\max}{}^+$	40	24	24	24
Δz^+	5	5	5	5
x_0	∞	−200	−200	−200

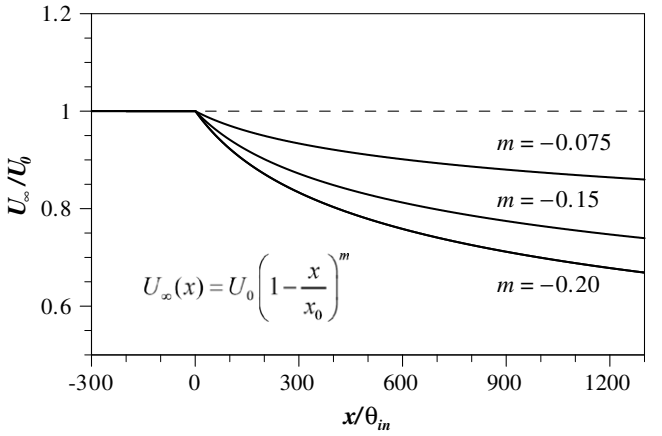

Fig. 2. Free-stream velocity distribution along the upper boundary of computational domain.

3. Results and discussion

3.1. Mean properties

First, we examine the variations of mean wall variables along the wall due to the APGs. Fig. 3 shows the streamwise distributions of the skin friction C_f and wall pressure coefficient C_p based on U_0 for systems with $m=-0.075$, -0.15 and -0.2. It is seen that, in each system, the boundary layer develops under a ZPG at the inlet and then the streamwise pressure gradient becomes strongly adverse. In each system, the skin friction decreases rapidly in the strong pressure gradient region ($dC_p/dx>0$, $dP^+/dx>0$), and then P^+ and C_f decrease slowly as the flow achieves a stable equilibrium state. Here, P^+ is the non-dimensionalized pressure gradient parameter in wall units, defined as $P^+=\nu(dP/dx)/\rho u_\tau{}^3$. C_f decreases with increasing pressure gradient. The lowest value of C_f, observed in the system with $m=-0.2$, is on the order of 1.1×10^{-3}, indicating that the flows examined here do not approach separation. In all of the flows, C_f decreases monotonically all the

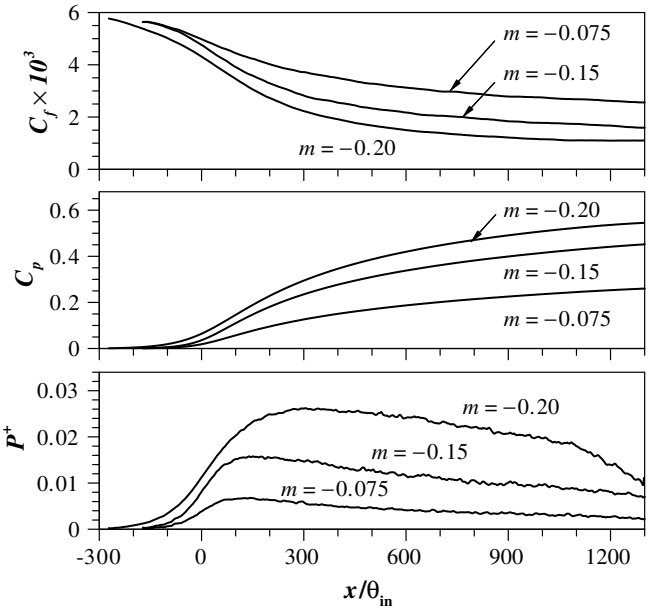

Fig. 3. Streamwise distributions of skin friction coefficient, pressure coefficient and non-dimensionalized pressure gradient parameter.

way to the end of the computational domain, consistent with the findings of Skote et al. (1998). However, this monotonic decrease stands in contrast to the experimental results of Skåre and Krogstad (1994), who reported that C_f becomes constant when the flow achieves a stable equilibrium state in the downstream region. This discrepancy may be due the lower Reynolds number used in our computations.

Clauser (1954) introduced the equilibrium parameters β and G which can be used to determine whether self-similarity has been achieved. The non-dimensionalized pressure gradient parameter β is defined as $\beta = (\delta^*/\tau_w)\,\mathrm{d}P/\mathrm{d}x$, and the shape factor G is defined as $G = (H-1)/(H\sqrt{C_f/2})$. Here δ^* is the displacement thickness, τ_w is the wall shear stress and H is the Kármán-type shape factor. The requirements for self-similarity are that both β and G should be

Table 2
Flow parameters

	m	β	G	Re_θ
Present	−0.075	0.25	8.13	850–1300
Skote et al.	−0.077	0.24	7.6	390–620
Present	−0.15	0.73	9.70	1000–1300
Skote et al.	−0.15	0.65	8.0–8.3	430–690
Bradshaw	−0.15	0.9	9	10,000–20,000
Present	−0.20	1.68	12.4	1200–1400
Skare and Krogstad	−0.22	20	29.6	40,000–50,000

constant along the streamwise direction. As shown in Fig. 4, β and G increase and then converge to constant values. Throughout this paper, we shall refer to this region of constant Clauser's parameters as the 'equilibrium region'. Table 2 lists the values of Clauser's parameters and the Reynolds number ranges in the equilibrium region for the three adverse pressure flows considered here. Note that β reaches a constant value sooner than G in all systems. This indicates that even though the balance between pressure gradient force and skin friction force remains unchanged as the flow moves downstream, self-similarity is not attained simultaneously and the mean velocity needs more streamwise length to be fully developed. The distance needed to achieve an equilibrium state increases with increasing m. Fig. 5 shows the velocity defect profiles at five locations along the streamwise direction in the equilibrium region for the systems with $m = -0.075$, -0.15 and -0.2. Here, the velocity is normalized by the friction velocity u_τ and defect thickness $\Delta = \delta^*\sqrt{2/C_f}$. The velocity defect profiles for the flows with $m = -0.075$, -0.15 and -0.2 almost coincide, indicating that self-similarity has been established in the present simulations.

Fig. 6 shows the mean velocity profiles normalized by wall units in the equilibrium region, along with the profile for the ZPG flow for comparison. The mean velocity profiles of the APG flows exhibit a large wake region. The linear law of the wall, $U^+ = y^+$, holds in the viscous sublayer ($y^+ < 5$) regardless of β. As β increases, the velocity profiles

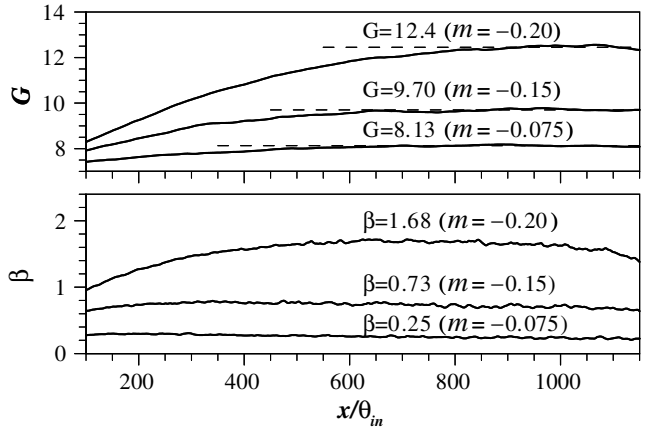

Fig. 4. Clauser's equilibrium parameters: non-dimensionalized pressure gradient parameters β and G.

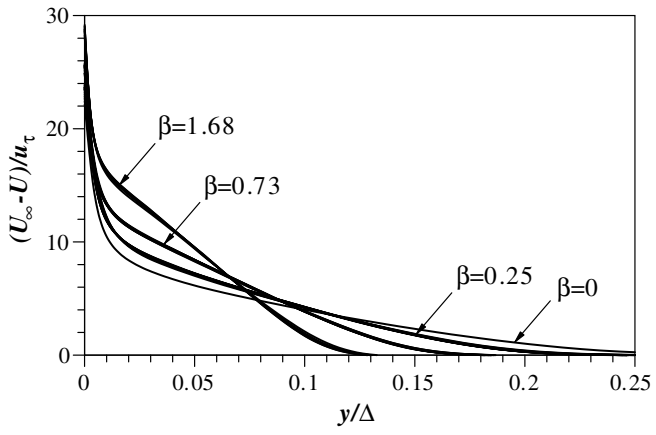

Fig. 5. Velocity defect profiles for five positions downstream in the equilibrium region.

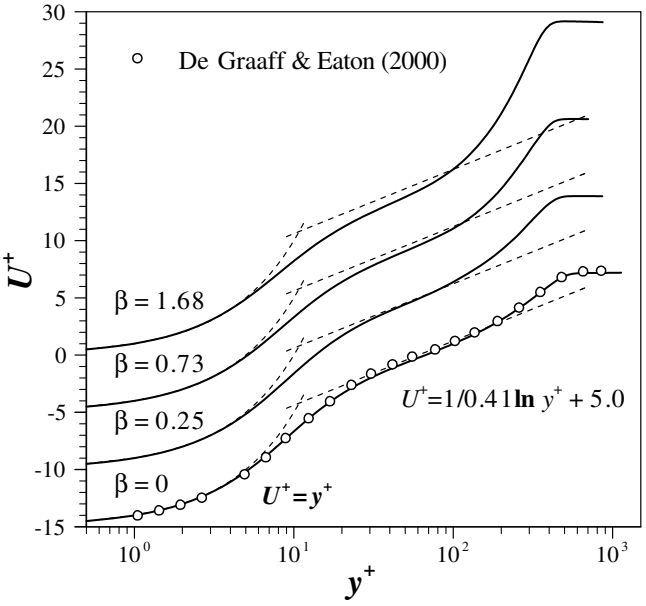

Fig. 6. Equilibrium mean velocity profiles in wall coordinates.

are shifted downward monotonically below the standard logarithmic law. Thus, the present results support previous reports on the failure of the standard logarithmic law of the wall in APG boundary layers (Nagano et al., 1993; Na and Moin, 1998; Spalart and Watmuff, 1993). A similar failure of the standard logarithmic law is seen in the non-equilibrium regions of the present spatially evolving flows (not shown here). Nagano et al. (1993) and Skåre and Krogstad (1994) found that the von Kármán constant κ of APGs was the same as that of the ZPG. However, the DNS studies by Coleman et al. (2003) and Spalart et al., 1986 showed that for an APG, the slope in the log region was higher than that of the ZPG. They conjectured that the discrepancy between their results and those of Nagano et al. (1993) and Skåre and Krogstad (1994) was that the latter authors had used higher Reynolds numbers. To isolate the effect of the APG and eliminate the effect of the Reynolds number, here we compare the slope in the log region at almost the same Reynolds number. The Reynolds numbers were chosen to be high enough that the von Kármán constant is almost 0.41 in the ZPG system ($Re_\theta > 900$, $Re_\tau > 360$). As seen in Fig. 7, the slope in the log region increases with increasing β. The starting point of the logarithmic law is lower in the APG systems than in the ZPG system ($y^+ \approx 30$), indicating that the slope in the log region depends not only on the Reynolds number but also the APG in the range of Reynolds numbers considered here. Much higher Reynolds numbers would be needed for Reynolds number to be the dominant factor determining the law between general and transient departure.

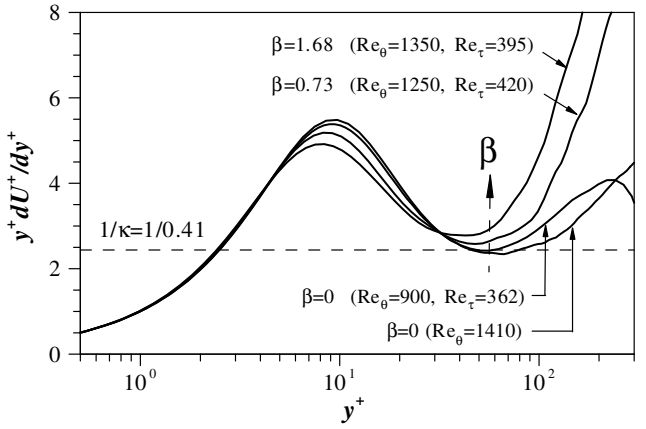

Fig. 7. Profiles of mean velocity derivative.

3.2. Second-order turbulent statistics

The presence of an APG significantly affects the turbulent flow statistics. The root-mean-square (r.m.s.) distributions of velocity fluctuations in the equilibrium region are shown in Fig. 8. The velocity fluctuations are normalized by wall units. All three components of the velocity fluctuations increase with increasing APG strength. In the inner region, the distributions of these components for different β values do not collapse to a single distribution, despite normalization by viscous wall units. The inner peak value of u_{rms}/u_τ increases with increasing β; however, the y-location of the inner peak remains unchanged as β is varied, and is similar to that of the ZPG system. An obvious difference between the APG flows and the ZPG flow is that in

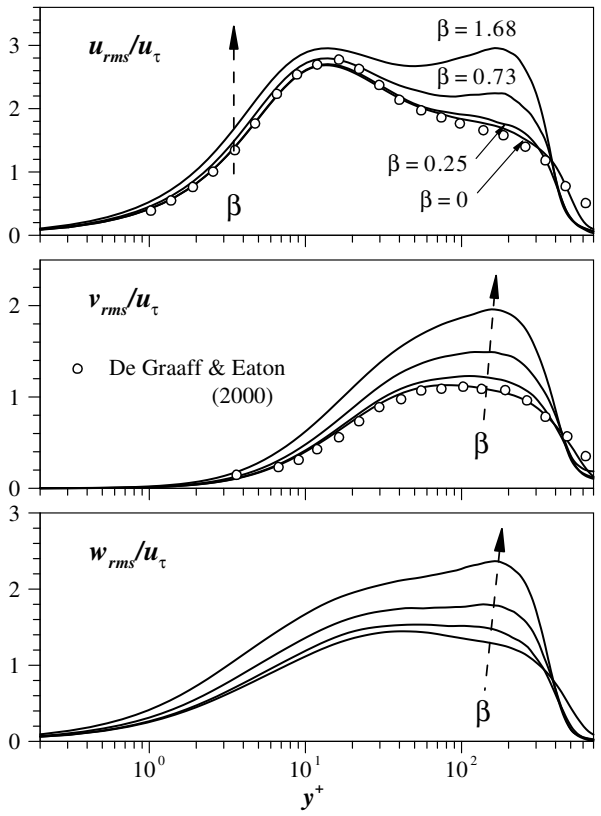

Fig. 8. Root-mean-square velocity fluctuations in the equilibrium region.

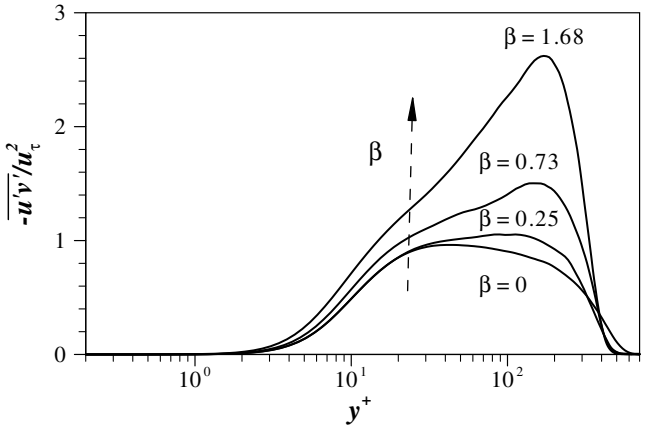

Fig. 9. Reynolds shear stress profiles in the equilibrium region.

the former systems, a second outer peak forms as β increases. For $\beta = 1.68$, the magnitude of the outer peak value is almost the same as that of the inner peak. The y-locations of peaks for v_{rms}/u_τ and w_{rms}/u_τ are similar to the outer peak of u_{rms}/u_τ and move away from the wall with increasing β. As shown in Fig. 9, the Reynolds shear stress, normalized by wall units, exhibits a trend similar to those observed for v_{rms}/u_τ and w_{rms}/u_τ. In the case of the Reynolds stresses, normalized by the local friction velocity, the peaks of maximum intensity develop in the outer region as β is increased.

Fig. 10 shows the distributions of r.m.s. velocity fluctuations for $m = -0.2$ at four streamwise locations ($x/\theta_{in} = 100$, 350 550 and 950) in the non-equilibrium region. Fig. 10a shows the velocity fluctuations normalized by the friction velocity, along with the experimental data of Nagano et al. (1993) for comparison. The calculated turbulence intensities in the present study are in good qualitative agreement with the experimental data. Initially, all three components of the turbulence intensity increase due to the strong APG as the flow moves downstream. After the pressure gradient has relaxed to the state required for equilibrium ($dP^+/dx < 0$), good similarity is observed in the inner region, although self-similarity of the mean velocity has not yet been attained. This inner self-similarity of the turbulence intensity is also valid for equilibrium flow. The y-locations and the values of the inner peak for u_{rms}/u_τ are almost the same irrespective of the streamwise location. However, the y-locations of the outer peak move away from the wall as the flow moves downstream. The y-locations of the peaks of v_{rms}/u_τ and w_{rms}/u_τ also move away from the wall. The development of the turbulence

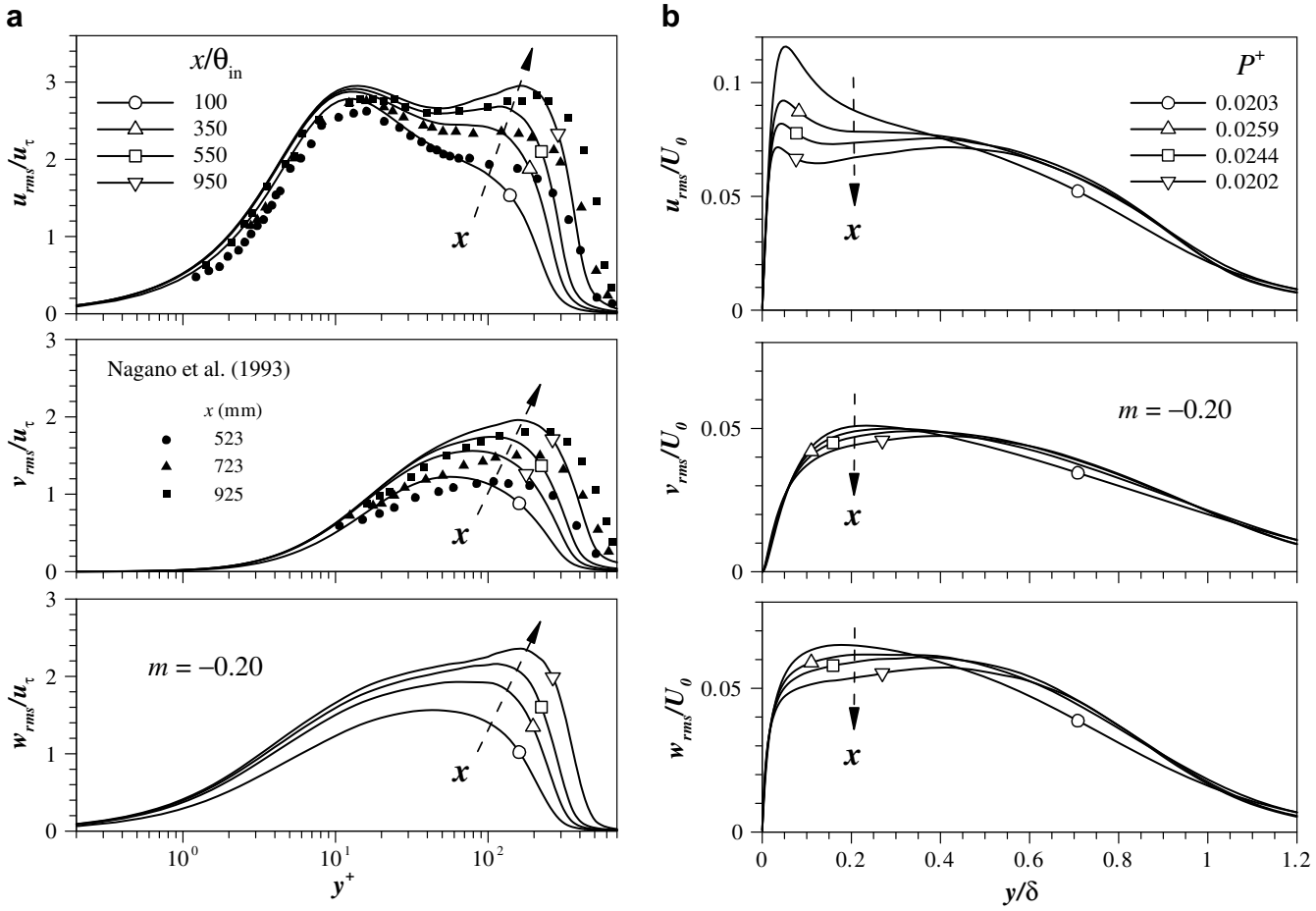

Fig. 10. Root-mean-square velocity fluctuations in the non-equilibrium region normalized by: (a) u_τ and (b) U_0.

intensities normalized by the free-stream velocity at the inlet U_0 is plotted in Fig. 10b. All of the calculated components of the velocity fluctuations in the inner region decrease with moving downstream, consistent with previous studies showing a reduction in the turbulence intensities normalized by the outer scale in the inner layer (Nagano et al., 1993). The amount of change in the velocity fluctuations near the wall increases in the order of u_{rms}, w_{rms}, v_{rms} (Nagano et al., 1993). In the outer region, the turbulence intensities initially increase, and the magnitude of this change increases with increasing β in the equilibrium state. After reaching the maximum value of P^+, the turbulence intensity profiles in the outer region do not change with APG strength whereas the mean velocity defect profiles continue to change. This behavior is obviously due to the non-equilibrium effect. These findings indicate that the outer turbulence of non-equilibrium APG flows may be unaltered (Nagano et al., 1993) or may increase (Debisschop and Nieuwstadt, 1996; Coleman et al. 2003) depending on the conditions of pressure or pressure gradient. The near-wall reduction in turbulence intensity propagates into the outer layer as the flow moves downstream. The Reynolds shear stress profiles in the non-equilibrium region are displayed in Fig. 11. The overall behavior of the Reynolds shear stress is similar to that observed in the wall-normal turbulence intensities; that is, the y-location of the maximum peak moves away from the wall.

3.3. Turbulent vortical structures

To observe the responses of outer vortical structures to an APG, we visualized the vortical structures ($y/\delta > 0.2$) in the equilibrium region using an iso-surface of swirling strength λ_{ci} (Zhou et al., 1999) (Fig. 12), where λ_{ci} is the imaginary part of the complex conjugate eigenvalue of the velocity gradient tensor. Examination of the swirling strength distribution assists in the detection of the cores of the vortical structures and in distinguishing vortical structures from shearing regions. Iso-surface values of

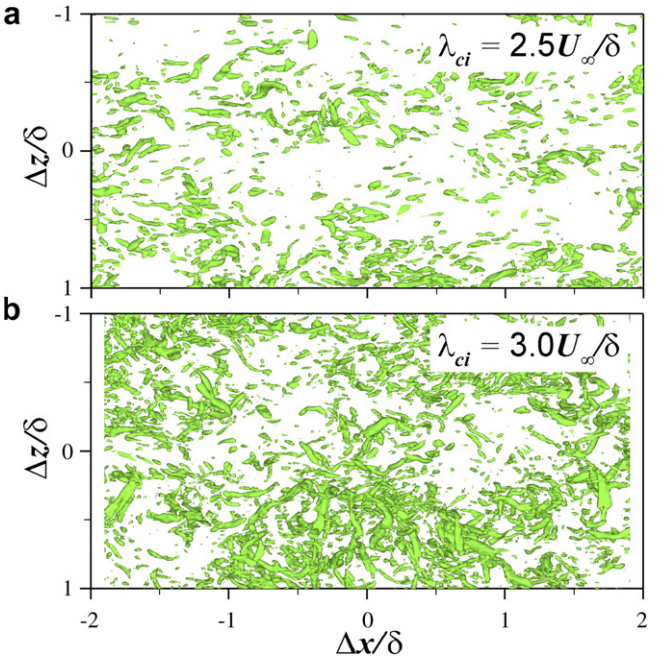

Fig. 12. Vortical structures in the outer layer ($y/\delta > 0.2$): (a) $\beta = 0$ and (b) $\beta = 1.68$.

$\lambda_{ci}\delta/U_\infty = 2.5$ and 3 were used for the ZPG and APG flows, respectively (Fig. 12a and b). Comparison of Fig. 12a and b clearly shows that the outer vortical structures are enhanced by the APG. Fig. 13 illustrates the distributions of r.m.s. vorticity fluctuations in the equilibrium region. As β increases, all of the components of the vorticity fluctuations (ω_x, ω_y and ω_z) decrease in the near-wall region and increase in the outer region. The increase in vorticity fluctuations in the outer region indicates the enhancement of the outer vortical structures by the APG. It is well known that vortical structures are closely related to the production of Reynolds shear stress (Robinson, 1991). The increase in Reynolds shear stress in the outer layer is likely due, at least in part, to the enhancement of outer vortical structures.

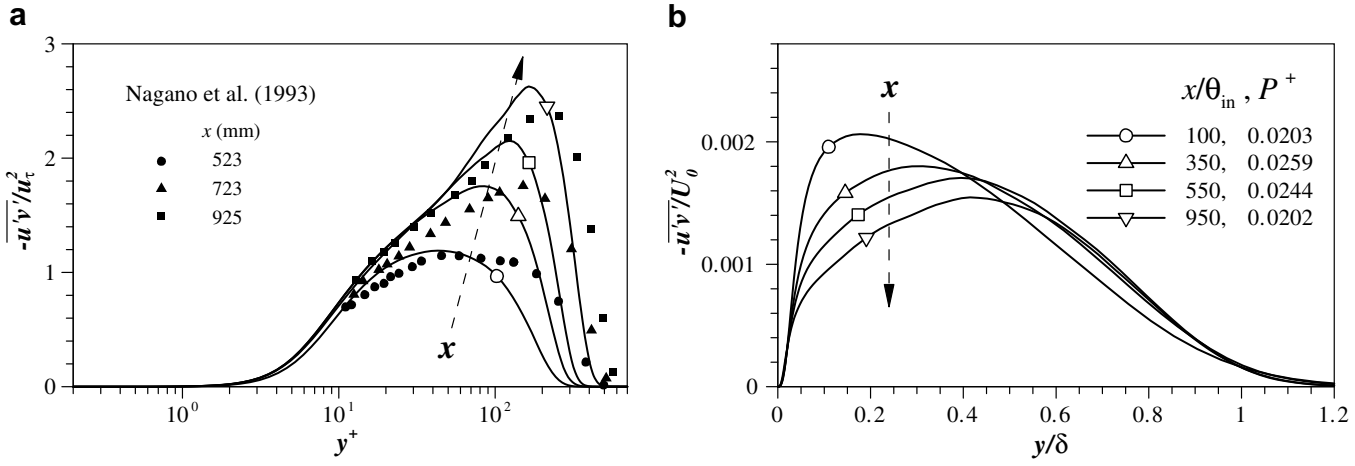

Fig. 11. Reynolds shear stress profiles in the non-equilibrium region normalized by: (a) u_τ and (b) U_0.

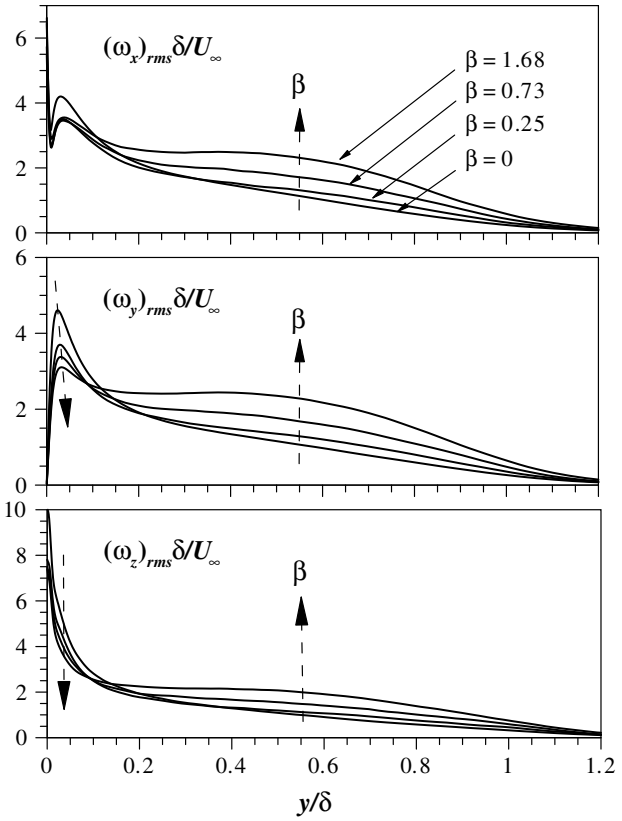

Fig. 13. Root-mean-square vorticity fluctuations in the equilibrium region.

Fig. 14 shows the root-mean-square pressure fluctuations, normalized by U_0, for $m = -0.2$ as a function of wall-normal distance. Initially, the pressure fluctuation profiles have one local maximum at around $y^+ \approx 30$. As the flow moves downstream, the y-location of the maximum remains unchanged, but the magnitude of the pressure fluctuations decreases. This reduction may be related to the weakening of the near-wall streamwise vorticity (Fig. 13). Kim (1989) reported that near-wall vortical structures contribute most to the generation of pressure fluctuations. The near-wall vortical structures are weakened by increasing the strength of the APG, and consequently the contribution of these structures to the source term in the Poisson equation decreases. As a result, the pressure fluctuations decrease in the near-wall region. As the flow moves downstream, the r.m.s. pressure fluctuation profiles develop another outer peak which subsequently becomes more dominant than the inner peak. The y-location of the outer peak moves away from the wall and is similar to the y-locations at which peaks were observed in the turbulence intensities and Reynolds shear stress (Figs. 8 and 9). This dominant outer peak may be partially due to the enhancement of the outer vortical structures by the APG.

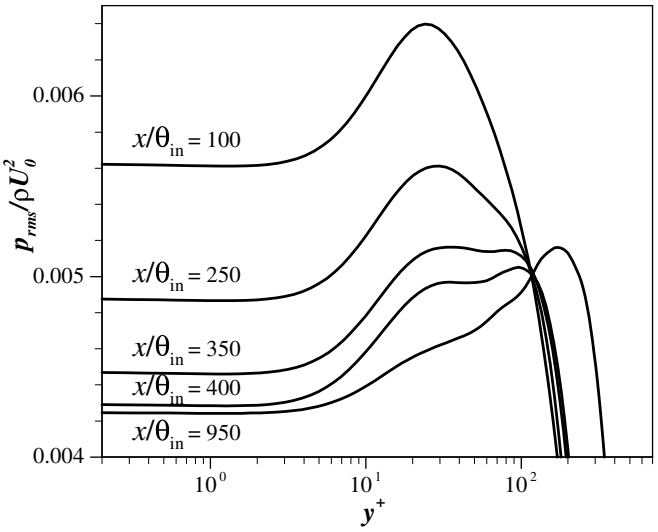

Fig. 14. Distribution of pressure fluctuations.

3.4. Reynolds stress budget

To see the effect of an APG on a turbulent boundary layer, we consider the budget of Reynolds stress equations:

$$\underbrace{\langle u_k\rangle \frac{\partial \langle u_i' u_j'\rangle}{\partial x_k}}_{\text{convection}} = \underbrace{-\overline{\left(\langle u_i' u_k'\rangle \frac{\partial \langle u_j\rangle}{\partial x_k} + \langle u_j' u_k'\rangle \frac{\partial \langle u_i\rangle}{\partial x_k}\right)}}_{\text{production}} \underbrace{-\frac{\partial \overline{u_i' u_j' u_k'}}{\partial x_k}}_{\text{turbulent transport}} \underbrace{-\frac{2}{\mathrm{Re}}\overline{\frac{\partial u_i'}{\partial x_k}\frac{\partial u_j'}{\partial x_k}}}_{\text{dissipation}} + \underbrace{\frac{1}{Re}\frac{\partial^2 \overline{u_i' u_j'}}{\partial x_k^2}}_{\text{viscous diffusion}} + \underbrace{\overline{p'\left(\frac{\partial u_i'}{\partial x_j} + \frac{\partial u_j'}{\partial x_i}\right)}}_{\text{pressure–strain}} \underbrace{-\frac{\partial \overline{p'(u_i'\delta_{jk} + u_j'\delta_{ik})}}{\partial x_k}}_{\text{pressure transport}} \tag{4}$$

where Eq. (4) is normalized by U_0^3/δ. Figs. 15 and 16 show the budgets for normal stresses and Reynolds shear stress in the equilibrium region. All of the terms near the wall in the Reynolds stress budget of a system with an APG are qualitatively similar to, or smaller than, those of the ZPG system. However, the budgets are significantly disturbed in the outer region, as shown in Figs. 15 and 16. The viscous diffusion terms are omitted in Figs. 15 and 16 since their contributions are restricted to the region very close to the wall. In the budget of $\overline{u'^2}$ of the APG flow with $\beta = 1.68$, the dominant second peak of the production term appears at around $y/\delta \approx 0.5$. This has been observed in many previous studies, such as that of Skåre and Krogstad (1994). This peak is mainly due to the high Reynolds shear stress in this region (Skåre and Krogstad, 1994). The magnitude of stress production for the APG flow is larger than that for the ZPG flow, and is in balance with the pressure–strain, dissipation and turbulent transport terms away from the wall. Note that on going from the ZPG to APG flow, the turbulent transport term increases in importance

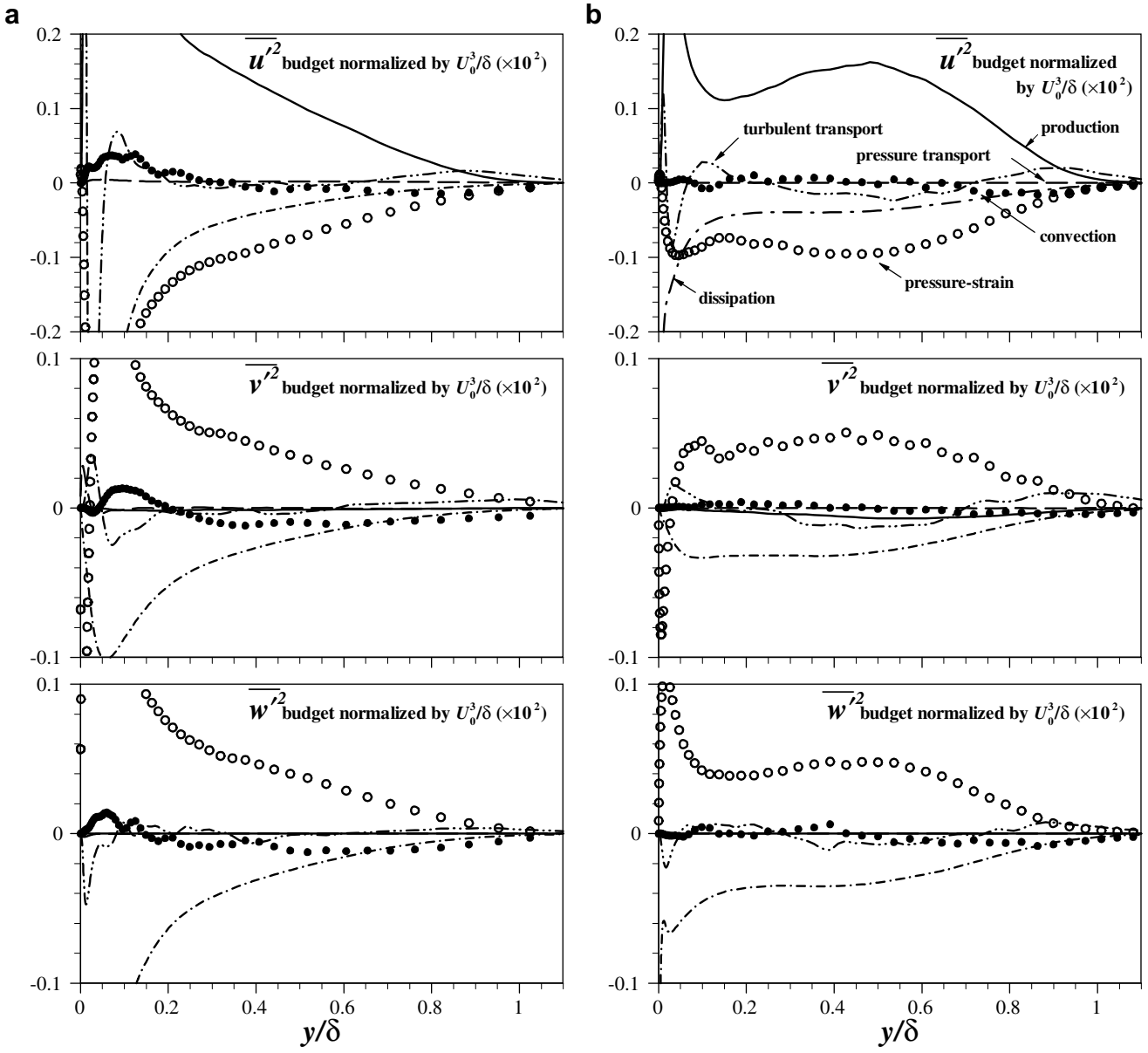

Fig. 15. Budgets for normal stresses in the equilibrium region normalized by U_0^3/δ: (a) $\beta = 0$ and (b) $\beta = 1.68$.

to a similar degree as the dissipation term. Fig. 17 shows the profiles of the time-averaged triple product term $\overline{v'u'^2}$ in the equilibrium region along with the experimental data of Houra et al. (2000). The profiles of $\overline{v'u'^2}$ in the log region decrease with increasing β. Finally, $\overline{v'u'^2}$ changes its sign from positive to negative on going from $\beta = 0.73$ to 1.68, as shown in Fig. 17, in qualitative agreement with the experimental data of Houra et al. (2000). The negative value of $\overline{v'u'^2}$ means that $\overline{u'^2}$ is transported by the turbulence toward the wall from the outer layer, which is the exact opposite of the behavior observed in the ZPG system. In the profiles of the pressure–strain term, the outer peak appears and the magnitude of this term increases in the outer region. In the budgets of $\overline{v'^2}$ and $\overline{w'^2}$, the dissipation terms are a dominant loss throughout the layer. The pressure–strain terms are dominant except in the vicinity of the wall. Similar to the budget of $\overline{u'^2}$, the pressure–strain terms of the APG flow have an outer peak and are larger than those of the ZPG flow far from the wall. The pressure–strain term is known to play a dominant role in energy redistribution among the components (Mansour et al., 1998). A negative sign of the pressure–strain term indicates transfer from this component to other components, whereas a positive sign denotes an energy gain. The increase in the pressure–strain term indicates that more energy is redistributed in the outer region under an APG than under the ZPG. The shear stress budgets in Fig. 16 are similar to those of $\overline{u'^2}$. The production and velocity pressure gradient terms $-\langle u\partial p'/\partial y + v\partial p'/\partial x\rangle$ show dominant gain and loss terms, respectively. The production term is in balance with the velocity pres-

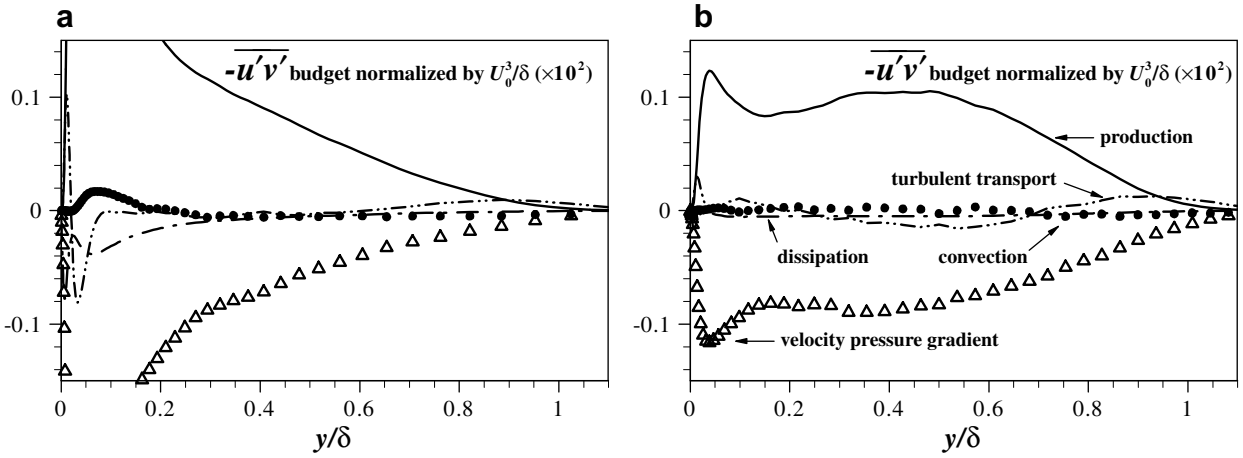

Fig. 16. Budgets for Reynolds shear stresses in the equilibrium region normalized by U_0^3/δ: (a) $\beta = 0$ and (b) $\beta = 1.68$.

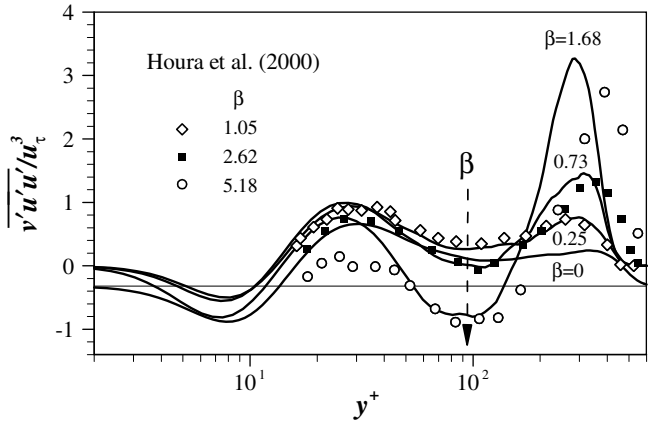

Fig. 17. Profiles of triple product $\overline{v'u'u'}$.

sure gradient term throughout most of the layer. This is in good agreement with the findings of Skåre and Krogstad (1994).

4. Summary and conclusions

In the present study, a detailed numerical analysis was performed to scrutinize the effects of an APG on a turbulent boundary layer. Statistical descriptions of flow quantities were obtained by performing DNSs of spatially developing turbulent boundary layer flows subjected to an APG. The equilibrium flows were established using a power-law free-stream distribution, $U_\infty \sim x^m$, and three equilibrium flows were simulated ($m = -0.075$, -0.15 and -0.2). For comparison, the ZPG system with $m = 0$ was also simulated. It was found that the Clauser pressure gradient parameter β converged sooner than did the shape factor G, indicating that the latter parameter required a greater streamwise distance to achieve self-similarity after attaining the force balance. As m increased, the distance needed to achieve self-similarity increased. The characteristics of the mean and r.m.s. quantities were in qualitative agreement with those of the Nagano group (Nagano et al., 1993). The simulation results support the conjecture that the standard logarithmic law of the wall is not valid for APG flows. The mean velocity in the logarithmic region fell below the logarithmic law with increasing the slope of the APG. For low Reynolds number flows, both the Reynolds number and pressure gradient were important determinants of the mean velocity in the logarithmic region. A DNS study using higher Reynolds numbers may be able to more clearly elucidate the validity of the standard logarithmic law of the wall for systems with an APG. As the flow relaxes to an equilibrium state, the turbulence intensities, normalized by the inlet free-stream velocity, collapsed well in the outer region. In the equilibrium region, the profiles of the mean velocity defect showed good self-similarity in the outer layer. The turbulence intensity and Reynolds shear stress profiles for the various APG systems collapsed well in the inner region when normalized by the friction velocity. The outer vortical structures, identified by λ_{ci}, were enhanced by the APG, which in turn led to an increase in the Reynolds shear stress. This caused the development of a second peak in the turbulent energy. The pressure fluctuation profiles also showed a second outer peak, which was of greater magnitude than the first inner peak. The effects of an APG on the redistribution of energy were investigated by examining the pressure–strain correlation tensor in the Reynolds stress budget. The amount of energy transfer from the streamwise velocity component to the other two velocity components was larger under an APG than under the ZPG. The inward turbulent energy transport in the APG flows, which is opposite to that of the ZPG flow, took place near the log region, which is consistent with previous experimental data.

Acknowledgements

The authors acknowledge the support of the Korea Institute of Science and Technology Information under the Grand Challenge Supercomputing Program.

References

Bernard, A., Foucaut, J., Dupont, P., Stanislas, M., 2003. Decelerating boundary layer: a new scaling and mixing length model. AIAA J. 41 (2), 248–255.

Bradshaw, P., 1967. The turbulent structure of equilibrium boundary layers. J. Fluid Mech. 29, 625–645.

Clauser, F.H., 1954. Turbulent boundary layers in adverse pressure gradients. J. Aerosol Sci. 21 (2), 91–108.

Coleman, G.N., Kim, J., Spalart, P.R., 2003. Direct numerical simulation of a decelerated wall-bounded turbulent shear flow. J. Fluid Mech. 495, 1–18.

Cutler, A., Johnston, J., 1989. The relaxation of a turbulent boundary layer in an adverse pressure gradient. J. Fluid Mech. 200, 367–387.

Debisschop, J.R., Nieuwstadt, F.T.M., 1996. Turbulent boundary layer in an adverse pressure gradient: effectiveness of riblets. AIAA J. 34, 932–937.

DeGraaff, D., Eaton, J., 2000. Reynolds number scaling of the flat plate turbulent boundary layer. J. Fluid Mech. 422, 319–346.

Houra, T., Tsuji, T., Nagano, Y., 2000. Effects of adverse pressure gradient on quasi-coherent structures in turbulent boundary layer. Int. J. Heat Fluid Flow 21, 304–311.

Inman, P.N., Bradshaw, P., 1981. Mixing length in low Reynolds number turbulent boundary layers. AIAA J. 19, 653–655.

Kim, J., 1989. On the structure of pressure fluctuations in simulated turbulent channel flow. J. Fluid Mech. 205, 421–451.

Kim, K., Baek, S.-J., Sung, H.J., 2002. An implicit velocity decoupling procedure for the incompressible Navier–Stokes equations. Int. J. Numer. Meth. Fluids 38, 125–138.

Le, H., Moin, P., Kim, J., 1997. Direct numerical simulation of turbulent flow over a backward-facing step. J. Fluid Mech. 330, 349–374.

Lee, J.-H., Sung, H.J., 2005. Response to a spatially developing turbulent boundary layer to a spanwise oscillating electromagnetic force. J. Turbul. 6 (39), 1–15.

Lund, T.S., Wu, X., Squires, K.D., 1998. Generation of turbulent inflow data for spatially-developing boundary layer simulations. J. Comput. Phys. 140, 233–258.

Mansour, N.N., Kim, J., Moin, P., 1998. Reynolds-stress and dissipation-rate budgets in a turbulent channel flow. J. Fluid Mech. 194, 1544.

Mellor, G.L., Gibson, D.M., 1966. Equilibrium turbulent boundary layers. J. Fluid Mech. 24, 225–253.

Na, Y., Moin, P., 1998. The structure of wall–pressure fluctuations in turbulent boundary layers with adverse pressure gradient and separation. J. Fluid Mech. 377, 347–373.

Nagano, Y., Tagawa, M., Tsuji, T., 1993. Effects of adverse pressure gradients on mean flows and turbulence statistics in a boundary layer. In: Durst, F., Friedrich, R., Launder, B.E., Schmidt, F.W., Schumann, U., Whitelaw, J.H. (Eds.), Turbulent Shear Flows, vol. 8. Springer, Berlin, pp. 7–21.

Robinson, S.K., 1991. Coherent motions in the turbulent boundary layer. Ann. Rev. Fluid Mech. 23, 601–639.

Skåre, P.E., Krogstad, P.-Å., 1994. A turbulent equilibrium boundary layer near separation. J. Fluid Mech. 272, 319–348.

Skote, M., Henkes, R.A.W.M., Henningson, D.S., 1998. Direct numerical simulation of self-similar turbulent boundary layers in adverse pressure gradient. Flow Turbul. Combust. 60, 47–85.

Spalart, P.R., Leonard, A., 1986. Direct numerical simulation of equilibrium turbulent boundary layers. In: Durst, F.J. et al. (Eds.), Turbulent Shear Flows, vol. 5. Springer, Ithaca.

Spalart, P.R., Watmuff, J., 1993. Experimental and numerical study of a turbulent boundary layer with pressure gradients. J. Fluid Mech. 249, 337–371.

Townsend, A.A., 1961. Equilibrium layers and wall turbulence. J. Fluid Mech. 11, 97–120.

Wilcox, D.C., 1993. Turbulence Modeling for CFD, Griffin.

Zhou, J., Adrian, J., Balachandar, S., Kendall, T.M., 1999. Mechanisms for generating coherent packets of hairpin vortices in channel flow. J. Fluid Mech. 387, 353–396.